Journal of Power Sources 262 (2014) 316–322

Contents lists available at ScienceDirect

Journal of Power Sources

journal homepage: www.elsevier.com/locate/jpowsour

# Durability of high performance Ni–yttria stabilized zirconia supported solid oxide electrolysis cells at high current density

Per Hjalmarsson [1], Xiufu Sun, Yi-Lin Liu, Ming Chen*

*Department of Energy Conversion and Storage, Technical University of Denmark, Frederiksborgvej 399, P.O. Box 49, DK-4000 Roskilde, Denmark*

## HIGHLIGHTS

- A Ni–YSZ supported SOEC cell with LSC–CGO oxygen electrode was tested.
- The test was carried out at −1 A $cm^{-2}$ and co-electrolysis conditions for 2700 h.
- The cell shows a record low initial ASR of 200 mΩ $cm^2$ at 800 °C.
- A record low degradation rate of ≤12 mV (or 0.9%)/1000 h at −1 A $cm^{-2}$ was achieved.
- The Ni–YSZ electrode partially reactivated under OCV.

## ARTICLE INFO

*Article history:*
Received 21 January 2014
Received in revised form
11 March 2014
Accepted 26 March 2014
Available online 1 April 2014

*Keywords:*
Solid oxide electrolysis cell
Co-electrolysis
Degradation
Mixed ionic electronic conductor

## ABSTRACT

We report the durability of a solid oxide electrolysis cell (SOEC) with a record low initial area specific resistance (ASR) and a record low degradation rate. The cell consists of a Ni–yttria stabilized zirconia (YSZ) cermet as support and active fuel electrode, a YSZ electrolyte, a gadolinia doped ceria (CGO) inter-diffusion barrier, and a strontium doped lanthanum cobaltite (LSC)–CGO composite oxygen electrode. The cell was tested at 800 °C and −1 A $cm^{-2}$ converting 31% of a 0.1:0.45:0.45 mixture of $H_2$:$H_2O$:$CO_2$ for approximately 2700 h, demonstrating an initial ASR of 200 mΩ $cm^2$ and a steady degradation rate of ≤12 mV (or 0.9%) per 1000 h. Electrochemical impedance spectroscopy (EIS) was used to study in situ changes in the electrochemical response of the cell and the retrieved data was treated to deconvolute resistive contributions from the physiochemical processes occurring within the cell. The results showed rapid initial fuel electrode degradation during the first 350 h followed by partial reactivation. The serial resistance was found to increase with time but in an exponentially decaying behavior. A discussion is made based on the detailed electrochemical results together with post-mortem microstructural analysis.



## 1. Introduction

Solid oxide electrolysis cell (SOEC) is an electrochemical device that can convert $H_2O$ or $CO_2$ into $H_2$ or CO using electrical energy and heat [1–4]. If both $H_2O$ and $CO_2$ are used as reactant gas to the fuel electrode (as the cathode in SOEC mode), the so-called syngas (mixture of $H_2$ and CO) is produced which can be further converted into various types of synthetic liquid fuels such as ethanol, dimethyl ether (DME) or synthetic diesel. This is advantageous from a storage point of view, due to their higher volumetric energy density as compared to for instance batteries. Moreover liquid fuels are more easily stored, transported and consumed using the current infrastructures [1–5]. Finally, if the electrical energy comes from renewable energy sources such as wind power or solar energy and the heat from waste heat produced in industrial processes, the entire fuel cycle can be considered $CO_2$ neutral.

In order to commercialize the SOEC technology an operational lifetime of at least 5 years is expected [5,6]. Degradation of SOECs has therefore been extensively studied under various conditions including steam electrolysis [7–10], $CO_2$ electrolysis [11] or co-electrolysis [12,13]. For a complete overview of reported SOEC degradation, the readers are referred to two recent review papers [14,15]. A number of different degradation mechanisms have been proposed depending on current density [7,9,12,16]. At current densities of 0–0.5 A $cm^{-2}$, it has been argued that impurity poisoning of the active sites at the Ni–yttria stabilized zircona

* Corresponding author. Tel.: +45 4677 5757; fax: +45 4677 5858.
*E-mail address:* minc@dtu.dk (M. Chen).
[1] Present address: Topsoe Fuel Cell A/S, Nymoellevej 66, DK-2800 Kgs. Lyngby, Denmark.

http://dx.doi.org/10.1016/j.jpowsour.2014.03.133
0378-7753/

(YSZ)/YSZ/gas triple phase boundaries (TPBs) is the main cause for degradation [10]. It has also been shown that this degradation mechanism can be avoided by careful cleaning of the feed stream before entering into the Ni–YSZ electrode compartment [17]. From an economic perspective it is beneficial to operate the cells at high current densities and low over-voltage in order to reduce both investment and production costs. It is therefore wishful to operate the SOEC at $\geq$1 A cm$^{-2}$. However, at such high current densities it has been reported that lateral cracks form within the 8 mol.% $Y_2O_3$ stabilized $ZrO_2$ (8YSZ) electrolyte causing an additional, and rather severe degradation process [7]. It was observed that inter-granular nano-pores form within YSZ close to the strontium doped lanthanum manganite (LSM: $La_{1-x}Sr_xMnO_3$)–YSZ composite oxygen electrode (as the anode in SOEC mode) as a result of high oxygen potentials on this side of the cell during strong electrolysis polarization.

In a recent publication [18] it was observed that replacing the LSM–YSZ oxygen electrode with mixed conducting $La_{0.6}Sr_{0.4}Co_{0.2}Fe_{0.8}O_{3-\delta}$ (LSCF) oxygen electrode together with an $Ce_{0.9}Gd_{0.1}O_{1.95}$ (CGO) inter-diffusion barrier layer reduced the degradation associated with both the serial and polarization resistance when operated at −1.5 A cm$^{-2}$. The reason for the observation is not yet fully understood but possible explanations are (1) the different material and microstructure of the inter-diffusion barrier within which the high oxygen potential was found or (2) higher oxygen exchange kinetics of the LSCF electrode.

Despite the improved stability of the SOEC with an LSCF oxygen electrode, high and continuously increasing degradation rates above 500 mV per 1000 h (500 mV khs$^{-1}$) was observed when operated at −1.5 A cm$^{-2}$ [18]. At electrolysis current densities at and below 0.5 A cm$^{-2}$, on the contrary, very stable performance has been observed with cleaned upstream to the fuel electrode [17]. Regarding current densities between −0.5 and −1.5 A cm$^{-2}$, only few results are reported from SOEC testing [19]. This study aims at analyzing and reporting the electrochemical results from a SOEC tested at −1 A cm$^{-2}$ and 800 °C under co-electrolysis conditions.

## 2. Experimental

A Ni–YSZ supported SOEC (here after named as the tested cell) was manufactured using a support (Ni–YSZ cermet, ~300 μm in thickness), a fuel electrode (Ni–8YSZ cermet, ~10 μm in thickness) and an electrolyte (8YSZ, ~10 μm in thickness). A CGO layer (~2 μm in thickness) was applied using physical vapor deposition (PVD) before an LSC–CGO (LSC = $(La_{0.6}Sr_{0.4})_{0.99}CoO_{3-\delta}$) oxygen electrode was screen printed and sintered. The cell has an active electrode area of 4 × 4 cm$^2$. The cell was tested in a SOFC test setup described elsewhere [20]. Gold and nickel meshes were used as current collector components on the oxygen and fuel side, respectively. The cell was sealed at its edges by glass. The flow compartments were sealed at 850 °C for 2 h prior to reduction. The Ni–YSZ electrode was reduced also at 850 °C in 9% $H_2$ in $N_2$ for 2 h followed by 1 h in humidified $H_2$ (with 4% $H_2O$).

The initial and final electrochemical characteristics of the cell were tested at 850, 800 and 750 °C. At each temperature *i*–*V* polarization (in both SOFC and SOEC polarization mode) and electrochemical impedance spectroscopy (EIS) measurements were carried out with both air and $O_2$ supplied to the LSC–CGO oxygen electrode and with a steam content of both 20% and 50% supplied to the Ni–YSZ fuel electrode. Flows were set to 50 l h$^{-1}$ of air/$O_2$ and 24 l h$^{-1}$ of $H_2/H_2O$. *i*–*V* polarization measurements were carried out under co-electrolysis condition with a 24 l h$^{-1}$ flow of oxidants ($X_F(CO_2) = 0.45$, $X_F(H_2O) = 0.45$, $X_F(H_2) = 0.1$, where the subscript F represents fuel electrode) and with 50 l h$^{-1}$ $O_2$ supplied to the LSC–CGO oxygen electrode. EIS measurements were carried out at zero DC current using a Solartron 1260 frequency analyzer and an external shunt in series with the cell. The spectra was recorded from 96,850 Hz to 0.08 Hz with 12 points per decade and corrected using the short circuit impedance response of the test setup. Impedance measurements were corrected for inductive contributions from the test setup using the method based on Kramer Kronig relations described in Ref. [21]. In this study, analysis of the impedance data was performed using impedance transforms in the software Ravdav [22].

In between the initial and final electrochemical characteristics, the electrochemical stability of the cell was tested in galvanostatic mode at −1 A cm$^{-2}$ and 800 °C with an inlet gas composition of $CO_2/H_2O/H_2$ = 45/45/10 and a reactant ($H_2O$ + $CO_2$) utilization of 31%. The 10% of hydrogen excess was added in order to avoid oxidation of the Ni in the Ni–YSZ electrode. The gas supplied to the Ni–YSZ electrode compartment were cleaned at 720 °C before being fed to the cell, following a procedure described by Ebbesen and Mogensen [17]. A flow of 50 l h$^{-1}$ of $O_2$ was supplied to the LSC–CGO electrode in order to ensure a stable $pO_2$ in the oxygen electrode compartment. EIS were recorded under current during the galvanostatic test. The applied current was accidentally cut after 1150 h test due to unforeseen technical reasons. The test was continued under the same condition right after the technical problem was solved. After the final electrochemical characterization, the cell was cooled to room temperature with 9% $H_2$ in $N_2$ supplied to the Ni–YSZ electrode compartment and air supplied to the LSC–CGO electrode compartment.

A nominally identical cell was used as reference (here after named as the reference cell) and performed initial electrochemical characterization only. The cell was primarily used to test the cell test reproducibility and as a reference for assessing the microstructural changes induced by the galvanostatic test. The initial electrochemical characteristics of the reference cell were identical to the galvanostatically tested cell and were therefore not included in this paper.

Both the galvanostatically tested cell and the reference cell were selected for microstructural examinations. Polished cross-sections along the fuel flow direction from gas inlet to gas outlet were prepared. A Carl Zeiss Supra 35 scanning electron microscope equipped with a field emission gun (FE-SEM) was used. For chemical analysis the Supra 35 is equipped with an X-ray Energy Dispersive Spectrometer (EDS) and a microanalysis software NSS (Thermo Fischer Scientific Inc.). The samples were carbon coated prior to imaging and EDS analysis which was carried out at an accelerating voltage of 15 kV.

## 3. Results and discussion

Fig. 1 plots the results from *i*–*V* polarization measurements of the cell recorded at 800 °C under co-electrolysis conditions before and after the durability test as well as the corresponding secant area specific resistance ($ASR_{SEC}$). The cell shows an initial $ASR_{SEC}$ of 0.20 Ω cm$^2$ at −1 A cm$^{-2}$, 800 °C under co-electrolysis conditions described in the experimental section. The low resistance, which to the best knowledge of the authors is a record low, is considered as a consequence of the use of an LSC–CGO oxygen electrode on a CGO inter-diffusion layer produced using PVD technology. LSC is well known for its good mixed ionic and electronic conducting (MIEC) properties and its high catalytic activity toward oxygen reduction [23]. The application of a dense CGO inter-diffusion barrier layer made by PVD further reduces the resistance by efficiently preventing Sr diffusion toward the YSZ electrolyte and formation of non-conducting $SrZrO_3$ [24]. After the long-term galvanostatic test, the $ASR_{SEC}$ at −1 A cm$^{-2}$ have increased to 325 mΩ cm$^2$, which yields an average degradation rate of 47 mΩ cm$^2$ khs$^{-1}$ over the

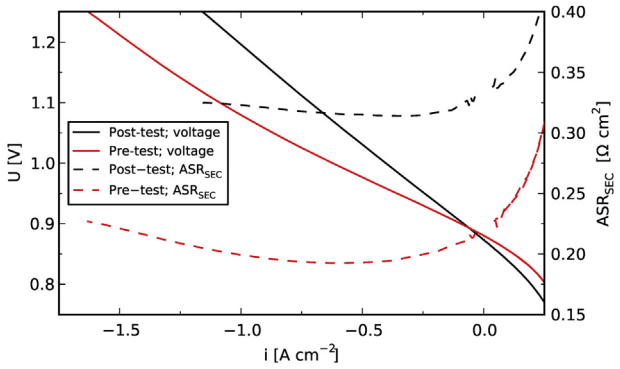


**Fig. 1.** $i$–$V$ polarisartion curves and the corresponding secant resistance measured under a 24 l $h^{-1}$ 45:45:10% flow of $H_2O$:$CO_2$:$H_2$ at 800 °C.

2650 h test period. Fig. 2 shows Nyquist plots of the inductance corrected impedance measured at open circuit voltage (OCV) under the same condition as in Fig. 1. The results suggest that the degradation is related to both the serial and polarization resistance of the cell. It should be noted that the $i$–$V$ and EIS plots of post-tests as plotted in Figs. 1 and 2 were not carried out directly after stopping the galvanostatic test but after a series of $i$–$V$ and impedance measurements at other gas compositions.

Fig. 3 plots the results from analyzing the EIS measurements before and after the durability test using the method of analysis of differences in impedance spectra (ADIS) when shifting the $pH_2O$ on the fuel electrode or the $pO_2$ on the oxygen electrode while keeping the other conditions constant [25]. The ADIS method allows distinguishing the frequency regime and the relative change in resistance of all processes dependent on the parameter used for this specific analysis ($pO_2$, $pH_2O$, $T$, etc). Gas shift ADIS is limited to analysis of electrode reactions that have a partial pressure dependence of the respective reactants and products which is the case for most of the electrochemical processes occurring in a SOEC. A stronger ADIS response after test for a given electrode can then be interpreted as an increase in resistance for this specific electrode reaction. As indicated by Fig. 3, the degradation of the fuel electrode is very weak as there is no major difference between the curves. The oxygen electrode appears to have degraded to some degree but the resistive contribution from this electrode is very small making quantitative assessment less accurate.

Fig. 4 plots the cell voltage curve of the galvanostatic test described in the experimental section. It also plots the corresponding $ASR_{SEC}$, calculated as $(OCV - U(t))/i$. The figure plots further the accumulated degradation rate calculated as $\overline{DR}(t) = (ASR_{SEC,t} - ASR_{SEC,t=0})/t$ where $t$ is the elapsed time since the start of the galvanostatic test. Finally, the figure plots the instantaneous degradation rate, calculated as the time derivative of $ASR_{SEC}$ ($dR/dt = \partial(ASR_{SEC,t})/\partial t$). In this plot we have applied a 150 h moving average filter over the calculated $dR/dt$ in order to linearize the degradation rate. The results show a rapid initial increase in cell voltage during the first approximately 350 h. After this

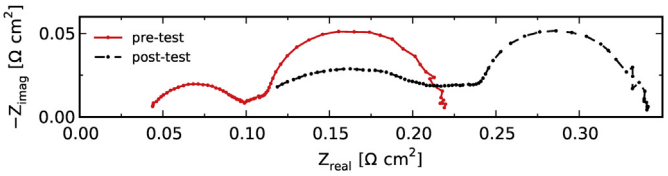


**Fig. 2.** Nyquist plots of EIS measurements at OCV and same conditions as in Fig. 1. The impedance has been corrected for lead inductance from the test setup.

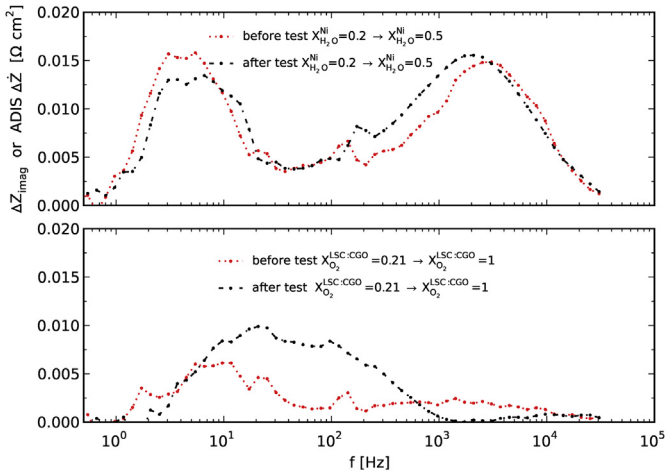


**Fig. 3.** Steam shift (top figure) and oxygen shift (bottom figure) ADIS analysis of the cell before and after the galvanostatic test.

period the cell voltage was found to increase only weakly with time. At about 1150 h into the test a power failure forced the cell to OCV. When operation was restored, the cell voltage returned to a lower value demonstrating that the accident actually had induced an instantaneous partial reactivation of the cell performance. After the power was restored the degradation behavior resembled the similar trends during the first 1000 h of the test with a relative high degradation during the first 300–400 h. This was followed by period of very low degradation which continued until the end of the test at 2650 h. The cell shows a steady degradation rate of ~12 mV (or 0.9%) $khs^{-1}$ evaluated from the measured cell voltage for the periods of 400–1000 and 2000–2600 h. So far only Schefold et al. has demonstrated comparable however still slightly higher

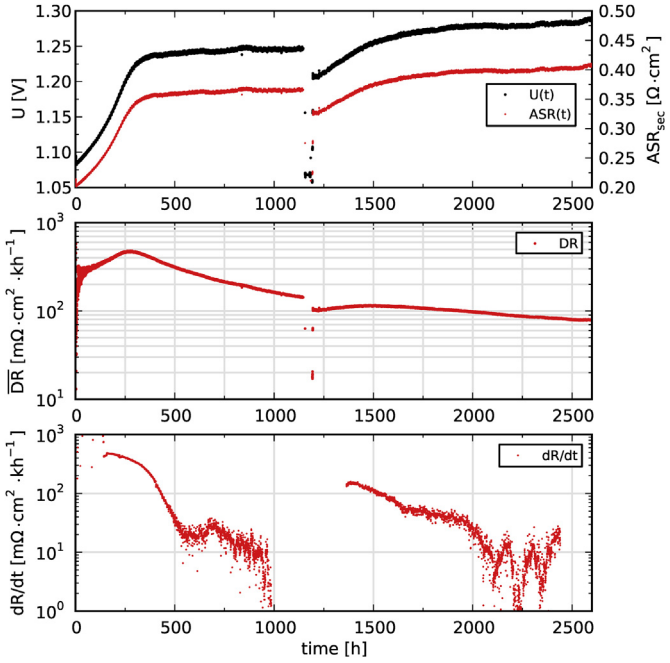


**Fig. 4.** Top: cell voltage and $ASR_{SEC}$ curves measured under conditions listed in the experimental section. Middle: accumulated degradation rate calculated as the change in $ASR_{SEC}$ from $t = 0$. Bottom: tangential degradation rate calculated as the time derivative of the $ASR_{SEC}$.

degradation rate (1.7% khs$^{-1}$ for the steady state degradation) also at −1 A cm$^{-2}$, but for electrolysis of steam and over 9000 h [26].

Over the entire testing period the cell temperature increased by approximately 6 °C. This shall result in a decrease of 5 mΩ cm$^2$ in the ASR$_{SEC}$ calculated using activation energy of 1.15 eV obtained during the electrochemical characterization before the test commenced. Taking this into account, the accumulated degradation rate for the entire test period of 2650 h reached ∼85 mΩ cm$^2$ khs$^{-1}$ with a final measured ASR$_{SEC}$ of 410 mΩ cm$^2$. This is substantially higher than the 325 mΩ cm$^2$ and corresponding degradation rate of 47 mΩ cm$^2$ khs$^{-1}$ determined from comparing $i$–$V$ polarization measurements before and after the test. The discrepancy indicates that the cell has recovered partially after the test stopped. The reason for this discrepancy is not yet clear. However, an interesting observation is that the cell also showed partial reactivation after the sudden power failure at 1150 h into the test. The results indicate that the SOEC can regain electrochemical performance by resting at OCV or being operated in SOFC mode for a period of time.

In order to estimate lifetime predictions the trend in the instantaneous degradation rate is of great importance. The calculated instantaneous degradation rate shows relatively large scatter, partly due to the impedance measurements that were recorded during the test. From Fig. 4 the d$R$/d$t$ is estimated to decrease toward an approximate rate of 5–10 mΩ cm$^2$ khs$^{-1}$ after the initial degradation leveled off. This rate is substantially lower than the measured average rates of 375 and 550 mΩ cm$^2$ khs$^{-1}$ reported in an aforementioned study of SOEC operated at −1.5 A cm$^{-2}$ under co-electrolysis flow [18].

In this work distribution of relaxation times (DRT) was applied in order to further understand the cell degradation behavior. Fig. 5 plots the analyzed DRT results, carried out at different $p$O$_2$ and $p$H$_2$O, temperatures and electrolysis currents during the initial characterization. The DRT method allows distinguishing the physiochemical processes that give rise to the impedance spectra of a SOEC provided that these processes have different characteristic time constants [2]. As shown in Fig. 5, upon changes in $p$H$_2$O at the Ni–YSZ side of the cell, three responses at 3–5 kHz, 20–40 Hz and 3–4 Hz respectively are clearly visible, of which only the high frequency process is strongly temperature dependent. Oxidation of H$_2$ at the Ni–YSZ triple phase boundaries of this cathode supported cell has previously been found to occur at around 3–5 kHz [3]. The same paper showed that gas diffusion impedance of H$_2$ and H$_2$O occurs at around 20 Hz, and that the conversion impedance, associated with Nernst potential perturbations due to changes in the $p$H$_2$/$p$H$_2$O ratio, occurs at 1–3 Hz. Fig. 5 distinguishes further two processes that depend on the $p$O$_2$ of the oxygen electrode side of the cell. The first occurs at an approximate summit frequency of 100–500 Hz depending on $p$O$_2$. This is the typical frequency regime within which the oxygen exchange reaction of LSC-based electrodes occurs [2,11]. The second response shows up at around 10 Hz when the $p$O$_2$ decreases below 0.21 atm. This is the typical frequency regime for diffusion of molecular O$_2$ on the oxygen electrode side [2]. Finally, there appears to be a response at 20–30 kHz which is not dependent on partial pressure change on either side of the cell. Previous studies have ascribed this process to ionic transport within the YSZ matrix of the Ni–YSZ electrode [4,5].

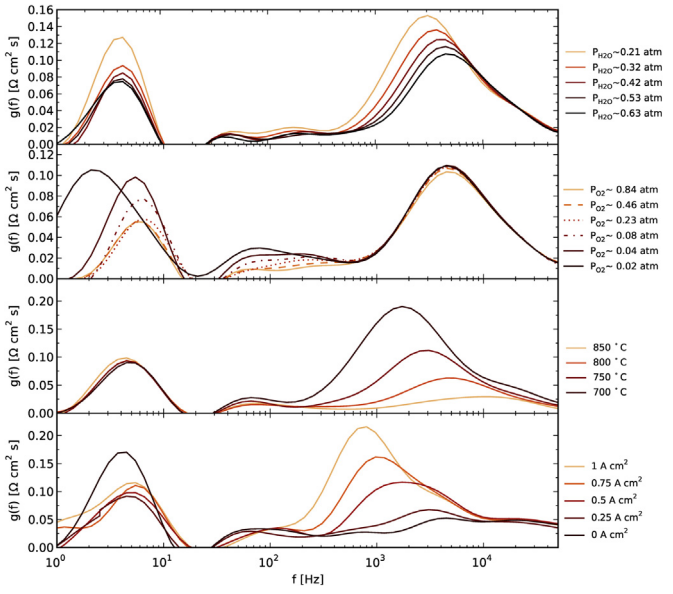


**Fig. 5.** DRT of impedance spectra recorded before the galvanostatic test as a function of (from top to bottom) a) $p$H$_2$O over the Ni–YSZ fuel electrode at OCV, $T$ = 700 °C, and with $X_O$(O$_2$) = 1; b) as a function of $p$O$_2$ over the LSC–CGO oxygen electrode at OCV, $T$ = 700 °C, and with $X_F$(H$_2$) = 0.50, $X_F$(H$_2$O) = 0.50; c) temperature, with $X_F$(H$_2$) = 0.80, $X_F$(H$_2$O) = 0.20; $X_O$(O$_2$) = 0.21; D) current density at $T$ = 800 °C and $X_F$(H$_2$) = 0.10, $X_F$(H$_2$O) = 0.45, $X_F$(CO$_2$) = 0.45, with $X_O$(O$_2$) = 0.50, and a total fuel flow rate of 24 l h$^{-1}$ and an oxygen flow rate of 50 l h$^{-1}$. The subscripts F and O represent fuel electrode and oxygen electrode, respectively.

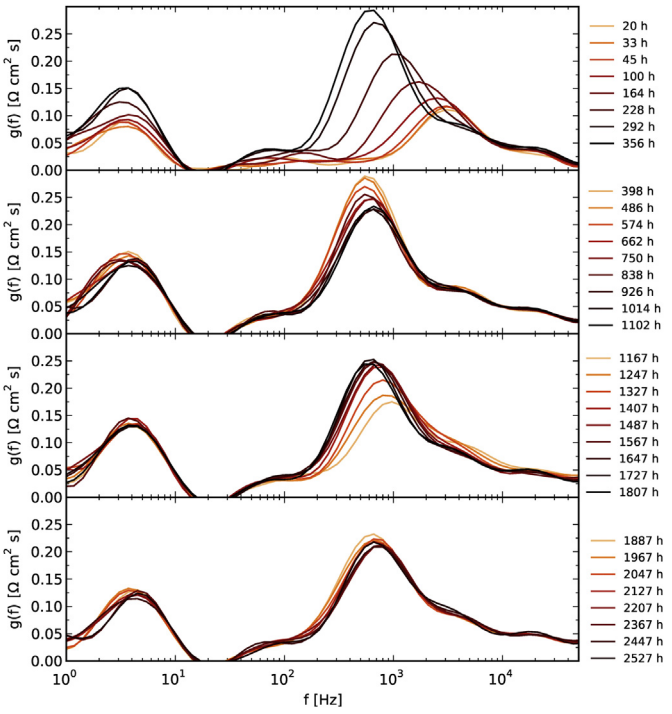


**Fig. 6.** DRT analysis of the impedance spectra measured during four different periods of the galvanostatic test.

Fig. 6 plots DRT analysis of EIS impedance during four different periods of the galvanostatic test. The first period from 0 to 350 h shows large increase in the main Ni–YSZ electrode response together with a shift in the summit frequency from 3 kHz to 500 Hz. A similar shift has been observed in previous studies, which has suggested this degradation to be related to poisoning of the Ni–YSZ TPB by impurities [6]. Additionally the conversion impedance at around 3–4 Hz appears to increase during this period. It is more difficult to conclude any trends in processes at 50–500 Hz as these processes are small and start to partially overlap with the response of the Ni–YSZ electrode. During the second period from 350 to 1100 h, a decrease in the Ni–YSZ response was observed indicating that the fuel electrode is partially reactivating. After the power cut,

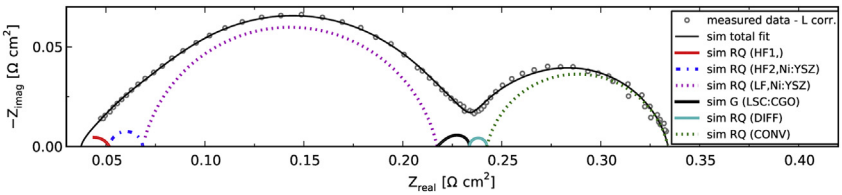


**Fig. 7.** Equivalent circuit (EQC) model of impedance measured during the galvanostatic test.

the impedance resistance of the Ni–YSZ electrode is again increasing for about 650 h. During the final period from 1900 h to the end of the test, the Ni–YSZ electrode appears to reactivate again albeit to a substantially lower degree than during the first period of reactivation.

From the DRT analysis in Fig. 5, two processes at frequencies higher than the main Ni–YSZ electrode response are observed. The first high frequency process is found at about 20 kHz and does not appear to change during the test. The second high frequency process is found at 3–5 kHz i.e. the frequencies at which the main Ni–YSZ process is nominally found. This process could in fact also be an integrated part of the impedance associated with the fuel oxidation. Whether this observed peak is related to an independent process or is part of a more complex and distributed impedance response is not yet fully resolved. In this paper, we have treated this response independently, mainly because from a degradation point of view it does not appear to be coupled to the main Ni–YSZ response.

Based on the DRT results, the impedance spectra were analyzed using the following equivalent circuit model: $L - R_S - (RQ)_{HF1} - (RQ)_{HF2} - (RQ)_{Ni:YSZ} - G_{LSC:CGO} - (RQ)_{DIFF} - (RC)_{CONV}$. Fig. 7 simulates, for a representative impedance spectra measured during the galvanostatic test, the different elements of the model.

The results from fitting the impedance spectra to the above described model are shown in Fig. 8. The model shows that the impedance spectrum is heavily dominated by the electrochemical processes related to the Ni–YSZ electrode and the $H_2O + CO_2$ conversion whereas the contribution from all the other processes is fairly small. Unfortunately, the main Ni–YSZ response overlaps partially with the oxygen electrode process and the $Z_{HF2}$ process. Additionally, the resistance of the oxygen electrode process and the $Z_{HF1}$ (this is the right legend not on the plot) and $Z_{HF2}$ are small compared to that of $Z_{Ni-YSZ}$. It is therefore difficult to accurately and quantitatively conclude trends in the resistance of these processes with time. It is for these reasons not possible to make detailed discussions and accurate conclusions on these four minor processes. The results from both DRT analysis as well as equivalent circuit fitting indicate that the LSC–CGO oxygen electrode appears not to suffer from any major degradation processes under the conditions in this test. In contrast to this the gas shift ADIS analysis of impedance measured before and after test shows that the oxygen electrode has suffered from degradation. Oxygen electrode degradation is demonstrated further by DRT analysis, shown in Fig. 9, which concludes an increase in the oxygen electrode resistance after test, although to a still comparatively small value. It also appears as though $R_{HF1}$ and in particular $R_{HF2}$ increase suddenly from 250 to 350 h into the test which is the period at which the resistance of the main Ni–YSZ process reaches its maximum. The high frequency response has previously been determined to be independent on changes in $pH_2O$ [27] which is why it is not possible to identify this process using gas shift ADIS. However, from Fig. 9 it is evident that a process occurring at 20–50 kHz has increased substantially during the test.

In addition, the following can be further deduced from Fig. 8:

- Passivation/activation of the Ni–YSZ electrode. The results from fitting the impedance data to an equivalent circuit model show, in agreement with the DRT analysis, an initial degradation on the Ni–YSZ electrode, followed by a partial reactivation. The degradation has previously been ascribed to poisoning of the TPBs at the fuel electrode by impurities such as silica [18]. It has been suggested further that reactivation of Ni–YSZ TPBs may occur due to crystallization of the silica phases [10]. Recent publications have also shown that Zr may dissolve into the nickel particles and expel as nano-particles at the nickel surface provided that the over-potential is high enough [28]. However the later degradation mechanism is not expected to be reversible upon restoring open circuit voltage.
- Strong coupling of the fuel electrode and fuel conversion impedance. During periods when the Ni–YSZ is degrading, the resistance associated with fuel conversion impedance is also observed to increase. The opposite is seen for the periods when the Ni–YSZ electrode is partially activating. The reason for this coupling is not yet understood.

Fig. 10 plots serial resistance degradation after the power cut, together with a fitted line using an exponentially decaying function

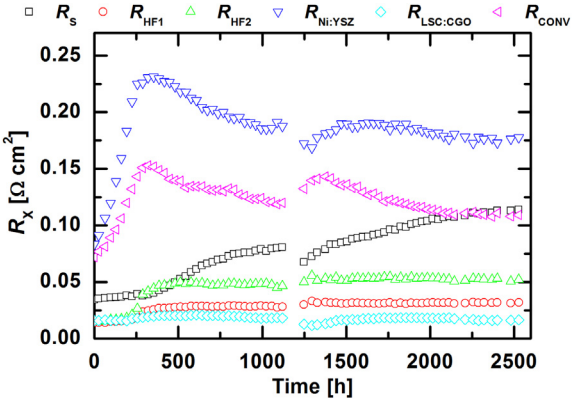


**Fig. 8.** Break down of losses by fitting the impedance spectra measured during the galvanostatic test to the equivalent circuit model shown in Fig. 7.

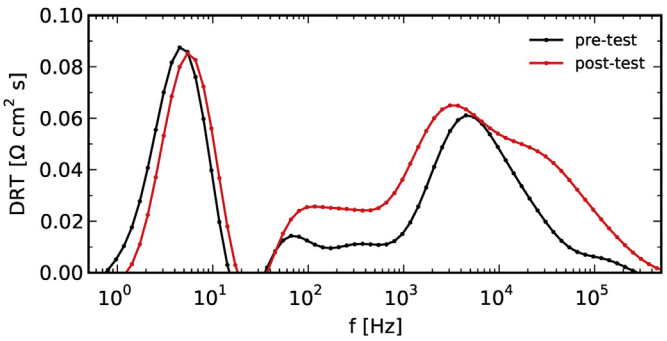


**Fig. 9.** DRT response of the EIS measured at OCV and 800 °C with $X_O(O_2) = 1$ and $X_F(H_2O) = 0.5$ before and after the galvanostatic test.

with an asymptotic limit of 125 mΩ cm$^2$. The major reason for the high degradation rates in previous tests has been a large increase in the serial resistance due to the crack propagation within the YSZ electrolyte [9,10,19]. The fact that the increase in the serial resistance is rather low for the cell in this test and that $R_S$ degradation appears to decay over time suggests that the cell is not suffering from the degradation mechanism proposed in Ref. [9].

The analysis of impedance measured at OCV before and after the galvanostatic test using ADIS and the analysis of impedance measured under current during test using DRT arrive at different conclusions with respect to the main Ni–YSZ electrode. The ADIS analysis shows that the main Ni–YSZ response has not suffered from almost any degradation whereas the DRT analysis highlights an extensive degradation (occurring rapidly during the initial phase of the test). In this context it could possibly be of importance that the post-test reported in Fig. 1, Figs. 2 and 3 were measured after a series of SOFC polarization measurements under various $pH_2O$ on the fuel side and $pO_2$ on the oxygen side of the cell. A hypothetical explanation could be that the Ni–YSZ recovers almost fully during the post-test measurements. A substantial reactivation of the Ni–YSZ electrode would also explain the discrepancy between the accumulated degradation rates calculated on the basis of pre- and post-test *i*–*V* measurements and on the basis of cell voltage at the start and end of the test.

SEM investigations were carried out along the fuel electrode flow direction from gas inlet to gas outlet of the tested cell and the reference cell. In the tested cell, mild microstructural degradation is found in the Ni–YSZ cathode, and the degradation occurs evenly in the entire cell from inlet to outlet. Hence, only the images taken from the center of the cell are presented in Fig. 11. The only noticeable microstructural changes in the tested cell were seen in the active Ni–YSZ electrode, namely the characteristic "dark ring" around some Ni grains (Fig. 11b). This could indicate the presence of Zr-oxide nano-particles on the surface of Ni grain, which has previously been identified as one of the major degradation mechanisms for Ni–YSZ electrodes under SOEC operation [28]. However, it is also noticed that this phenomena is limited to only a few Ni grains along the electrolyte-fuel electrode interface in contrast to the [28] where the degradation from Zr-oxide particles was found to be more severe. This is in good agreement with the results obtained from electrochemical characterizations which show relatively mild degradation when comparing the electrochemical performance of the cell before and after the test.

For the oxygen side, SEM examinations have not found any noticeable microstructural change in the YSZ electrolyte or in the CGO barrier layer. There could be microstructural changes in the LSC–CGO anode, but beyond the detection limit of SEM. As shown in Fig. 11b, the adhesion between the different layers (electrolyte, barrier layer, and oxygen electrode) of the tested cell remains relatively intact after 2600 h's testing. Small gaps (a few hundreds of nm, not shown here) are occasionally seen between the oxygen

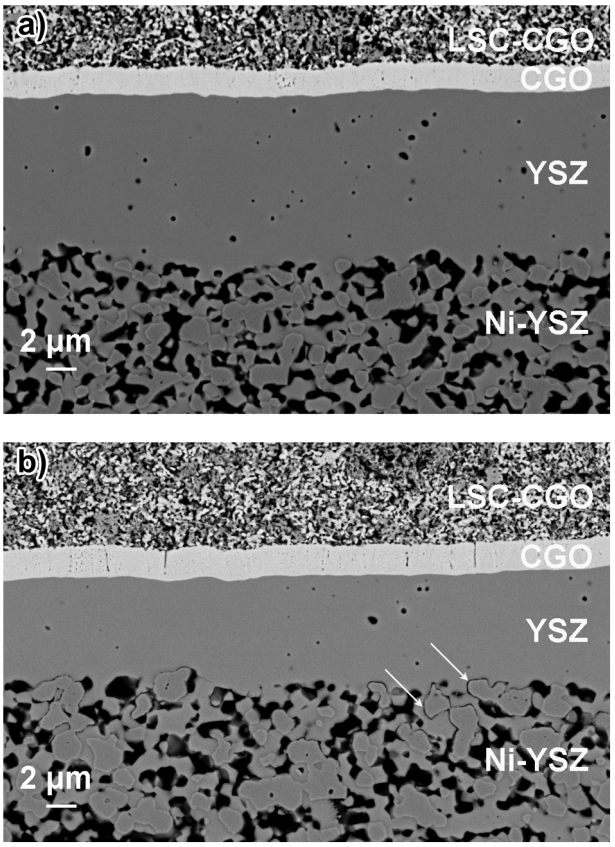


**Fig. 11.** SEM back-scattered images showing the cross-sections of (a) the reference cell, (b) the tested cell. Examples of the "dark ring" around Ni grains are indicated by the white arrows in Fig. 11b.

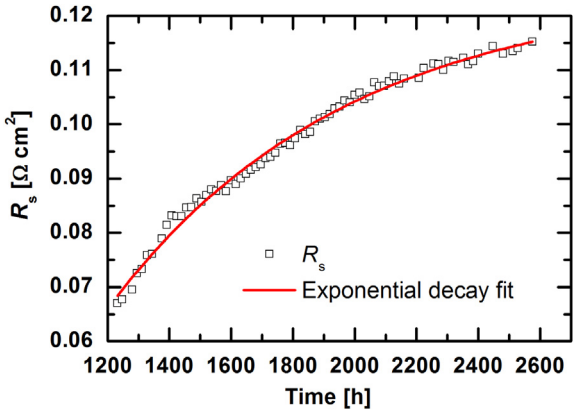


**Fig. 10.** Trend in the serial resistance with time for the period after the power cut till end of the test.

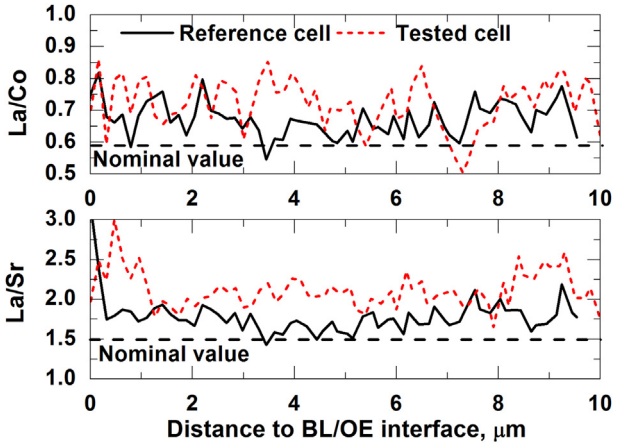


**Fig. 12.** Atomic ratios of La/Co and La/Sr evaluated from EDS line-scan results. The line-scans were made perpendicular to the barrier layer–oxygen electrode interface and further into the LSC/CGO oxygen electrode. The dashed lines in the figure were calculated nominal values according to the LSC powder composition $(La_{0.6}Sr_{0.4})_{0.99}CoO_{3-\delta}$.

electrode and the barrier layer. Such gaps are not necessarily caused by long-term galvanostatic testing, as they are also seen in the reference cell. EDS line-scan analysis was performed in the LSC–CGO anode and atomic ratios of La/Sr and La/Co were plotted as a function of the distance from the anode-barrier interface (Fig. 12). It shows that there is Sr- and Co-depletion in a region in the LSC–CGO anode of the tested cell, which is around 3–5 μm from the anode-barrier interface. Such depletion of Sr or Co was however not found in the reference cell indicating that the depletion of Sr and Co is a result of electrolysis.

## 4. Conclusion

The long-term durability of an anode supported SOEC with an inter-diffusion barrier layer of CGO produced using PVD and a screen printed LSC–CGO oxygen electrode has been tested at −1 A $cm^{-2}$, 800 °C and 31% conversion of a 50:50% $H_2O$:$CO_2$ mixture (co-electrolysis). The cell measured excellent initial performance with an ASR of 0.2 Ω $cm^2$. The cell was found to degrade rapidly during the first 350 h after which the degradation slowed down to an approximate rate of 5–10 mΩ $cm^2$ $khs^{-1}$. Four interesting observations were made: Firstly, the cell appears to partially reactivate its electrochemical performance when the electrolysis current is turned off and the cell is returned to OCV. The same observation was made from electrochemical post-test analysis. Secondly, the Ni–YSZ electrode was found to partially reactivate after an initial period of rapid degradation. Thirdly, the impedance of the oxidant reduction at the Ni–YSZ electrode appears to be apparently linked to the fuel conversion impedance. And fourthly, the serial resistance degradation was found to be relatively low and decays relatively exponentially with time, in contrast to previous tests at even higher current densities.

## Acknowledgment

This work was financially supported by Energinet.dk through the project ForskEL 2011-1-10609 “Development of SOEC cells and stacks”.

## References

[1] S.H. Jensen, P.H. Larsen, M. Mogensen, Int. J. Hydrogen Energy 32 (2007) 3253–3257.
[2] Z. Zhan, W. Kobsiriphat, J.R. Wilson, M. Pillai, I. Kim, S.A. Barnett, Energy Fuels 23 (2009) 3089–3096.
[3] S.D. Ebbesen, C. Graves, M. Mogensen, Int. J. Green Energy 6 (2009) 646–660.
[4] J. Hartvigsen, S. Elangovan, L. Frost, A. Nickens, C. Stoots, J. O'Brien, J.S. Herring, ECS Trans. 12 (2008) 625–637.
[5] C. Graves, S.D. Ebbesen, M. Mogensen, K.S. Lackner, Renew. Sust. Energy Rev. 15 (2011) 1–23.
[6] Q.X. Fu, C. Mabilat, M. Zahid, A. Brisse, L. Gautier, Energy Environ. Sci. 3 (2010) 1382–1397.
[7] R. Knibbe, M.L. Traulsen, A. Hauch, S.D. Ebbesen, M. Mogensen, J. Electrochem. Soc. 157 (2010) B1209–B1217.
[8] G. Schiller, A. Ansar, M. Lang, O. Patz, J. Appl. Electrochem. 39 (2009) 293–301.
[9] M.A. Laguna-Bercero, R. Campana, A. Larrea, J.A. Kilner, V.M. Orera, J. Power Sources 196 (2011) 8942–8947.
[10] A. Hauch, S.D. Ebbesen, S.H. Jensen, M. Mogensen, J. Electrochem. Soc. 155 (2008) B1184–B1193.
[11] S.D. Ebbesen, M. Mogensen, J. Power Sources 193 (2009) 349–358.
[12] C. Graves, S.D. Ebbesen, M. Mogensen, Solid State Ionics 192 (2011) 398–403.
[13] S.D. Ebbesen, C. Graves, A. Hauch, S.H. Jensen, M. Mogensen, J. Electrochem. Soc. 157 (2010) B1419–B1429.
[14] A. Nechache, M. Cassir, A. Ringuede, J. Power Sources 258 (2014) 164–181.
[15] P. Mocoteguy, A. Brisse, Int. J. Hydrogen Energy 38 (2013) 15887–15902.
[16] A.V. Virkar, Int. J. Hydrogen Energy 35 (2010) 9527–9543.
[17] S.D. Ebbesen, M. Mogensen, Electrochem. Solid State Lett. 13 (2010) D106–D108.
[18] P. Hjalmarsson, X.F. Sun, Y.L. Liu, M. Chen, J. Power Sources 223 (2013) 349–357.
[19] X.F. Sun, M. Chen, Y.L. Liu, P. Hjalmarsson, S.D. Ebbesen, S.H. Jensen, M.B. Mogensen, P.V. Hendriksen, J. Electrochem. Soc. 160 (2013) F1074–F1080.
[20] M. Mogensen, P.H. Larsen, P.V. Hendriksen, B. Kindl, C. Bagger, S. Linderoth, in: S.C. Singhal, M. Dokiya (Eds.), Solid Oxide Fuel Cells (SOFC VI), Electrochemical Society Inc., Pennington, 1999, pp. 904–915.
[21] B.A. Boukamp, J. Electrochem. Soc. 142 (1995) 1885–1894.
[22] C. Graves, RAVDAV Data Analysis Software, Version 0.9.7, 2012.
[23] A. Petric, P. Huang, F. Tietz, Solid State Ionics 135 (2000) 719–725.
[24] R. Knibbe, J. Hjelm, M. Menon, N. Pryds, M. Sogaard, H.J. Wang, K. Neufeld, J. Am. Ceram. Soc. 93 (2010) 2877–2883.
[25] S.H. Jensen, A. Hauch, P.V. Hendriksen, M. Mogensen, N. Bonanos, T. Jacobsen, J. Electrochem. Soc. 154 (2007) B1325–B1330.
[26] J. Schefold, A. Brisse, F. Tietz, J. Electrochem. Soc. 159 (2012) A137–A144.
[27] A. Leonide, V. Sonn, A. Weber, E. Ivers-Tiffee, J. Electrochem. Soc. 155 (2008) B36–B41.
[28] M. Chen, Y.L. Liu, J.J. Bentzen, W. Zhang, X.F. Sun, A. Hauch, Y.K. Tao, J.R. Bowen, P.V. Hendriksen, J. Electrochem. Soc. 160 (2013) F883–F891.